Kinetics of the Oxidation of Iron Carbide Dispersed in a Carbon Matrix with Water Vapor

Walerian Arabczyk, Ewa Ekiert,* and Roman Jędrzejewski

Institute of Chemical and Environment Engineering, West Pomeranian University of Technology, Pułaskiego Street 10, 70-322 Szczecin, Poland

Received: October 28, 2008; Revised Manuscript Received: January 28, 2009

The reaction of iron carbide embedded in a carbon matrix with water vapor was studied in the temperature range 300−500°C and the partial pressure of water vapor p_{H_2O} = 0.63−3.26 kPa. At these conditions the superfine magnetite and hematite are the products of this reaction. High oxidation temperature and low partial pressure of water vapor are favorable conditions to obtain only magnetite phase dispersed in a carbon matrix. The oxidation rate of iron and iron carbide is the same for both of them in the initial, kinetic stage of the reaction. It was observed that carbon deposit caused an increase in the reaction rate as a result of spillover effect. The oxidation rate of iron carbide distributed in a carbon matrix increases linearly with the carburization degree of the sample. The reaction rate is also linearly dependent on the partial pressure of water vapor. The apparent activation energy was determined as 110 kJ/mol.

Introduction

The reaction of iron with steam is known as a process that can be useful for hydrogen production. It is a cyclic process, performed in two stages, in two reactors. In one of them the reaction of sponge iron with water vapor is performed to obtain hydrogen stream and iron oxides (hematite, magnetite, or wustite). The solid product, iron oxides, is transported to the second reactor and there it is reduced to metallic iron with a reducing gas such as carbon monoxide, syngas, or biomass gas. If the reducing mixture contains carbon compounds, then carbon deposit and iron carbide can also be formed.[1–4]

Nanocrystalline iron can also be used to produce hydrogen by means of catalytic decomposition of methane, or other hydrocarbons. It is also a cyclic process performed in two stages. Hydrogen-rich gas is obtained during carburization of sponge iron to form iron carbide and carbon deposit. Subsequently carbon products are burned and iron oxides are formed, which are reduced to metallic iron using methane/hydrocarbon.[5]

In both processes iron carbide is produced directly as the intermediate product or impurity. Next, it is exhibited to the atmosphere of oxidizing agent to produce iron oxide. If water vapor is used, then hydrogen is formed simultaneously. There is a huge interest among scientists in iron carbide because of the possibility of its application as hydrogen storage, generation, and transportation.[6] There are many papers on how to obtain iron carbide,[7–12] but the interactions of iron carbide with gases, which can be present in stored hydrogen atmosphere, are not well known.

Akiyama et al. studied the reaction between iron carbide and steam to produce gas mixture with high hydrogen concentration. They ascertained that iron carbide reacts with water vapor at a much lower temperature than thermodynamically expected. Moreover, they reported that iron carbide reacts with water vapor in the temperature range of 550−1000°C in two stages, with generating intermediate iron in the first step which is further oxidized to iron oxide.[13–15]

The kinetics of iron carbide oxidation with water vapor to obtain magnetite has never, as yet, been reported, and this is the main goal of this paper. Iron oxides are formed during the reaction of iron carbide with water vapor.[16] In this work the preparation of superfine particles of iron oxides (Fe_3O_4, 40 nm; α-Fe_2O_3, 60 nm) dispersed in carbon matrix is also presented.

Experimental Section

The investigations were performed over nanocrystalline iron, which was obtained by reduction of an alloy prepared by fusion of magnetite with a small amount of promoter oxides: Al_2O_3, CaO in a resistance furnace. Aluminum and calcium oxides were added to stabilize the nanocrystalline structure of iron at elevated temperatures. They do not create individual domains, but they are built into magnetite particles and after reduction process they are wetting the surface of iron.[17] The chemical composition of the sample was determined using inductively coupled plasma atomic emission spectroscopy (AES-ICP). The reduced samples contained 3.0 wt % CaO, 2.9 wt % Al_2O_3, and the rest iron. The obtained alloy was crushed and sieved to obtain a fraction of 1−1.2 mm.

The kinetics experiments were performed in a differential flow reactor with ideal mixing. Mass changes of the sample vs time were monitored using a thermogravimetric method. The grains of passivated nanocrystalline iron were placed as a single layer on a platinum basket hung in the reactor. The protecting oxide layer was polythermally reduced at a temperature rising from room temperature up to 660°C at a rate of 10°C/min under hydrogen flow and next isothermally at this temperature until the mass of the analyzed sample was stable. When the reduction was complete, an appropriate process was subsequently started. In the first step of the formation of nanocrystalline magnetite in carbon matrix, nanocrystalline iron was carburized with pure methane at 660°C to achieve the planned carburization degree (expressed as the ratio of carbon and iron masses in a sample). A series of iron carbide samples in a carbon matrix was obtained in this way, with carburization degree in the range of m_C/m_{Fe} = 0−2 g of C/g of Fe. Directly after carburization of the raw material, the mixture of carbon and iron carbide was cooled under nitrogen flow to the temperature in the range of

* Corresponding author: fax, +48914494686; phone, +48914494872; e-mail, edabrowa@ps.pl.

10.1021/jp809518b CCC: $40.75
Published on Web 04/01/2009

300−500°C, in which the examined process was performed. The oxidation process was initiated by the replacement of pure nitrogen with an oxidation mixture of nitrogen saturated with water vapor (p_{H_2O} = 0.63−3.26 kPa). Owing to the used size fraction of catalyst grains and linear rate of flow, the diffusion was not the reaction rate limiting step.

The phase composition of the samples after the reduction, carburization, and oxidation process as well as the average crystallite size were determined using the X-ray diffraction method. The patterns were performed using a Cu $K\alpha_1$ radiation (diffractometer X'Pert PRO Philips).

The average crystallite size was calculated with the help of the Scherrer's equation shown below[18]

$$D = \frac{k\lambda}{\beta \cos \theta} \quad (1)$$

where D is the average crystallite size, k is Sherrer's constant which equals approximately 1, λ is the wavelength of the used X-ray radiation, β is the difference of the measured half peak intensity width and apparatus correction, and θ is the position of peak maximum.

The graphitization degree of carbon in the samples was calculated by means of the Maire and Mering formula[19]

$$g = \frac{3.44 - 0.1d}{0.086} \times 100\% \quad (2)$$

where g is the graphitization percentage and d is the interplane distance C(002) in nanometers.

The content of carbon in the samples was determined using Total Carbon method. The sample was burned and carbon dioxide was analyzed using IR spectroscopy (Multi N/C 2000 Analytik Jena).

Results and Discussion

The reaction rate can be described as a function of temperature, partial pressure of water vapor, relative increase of oxygen mass, expressed as oxygen mass gain divided by mass of iron in a sample, and a degree of iron carburization, expressed as carbon mass gain divided by mass of iron in a sample. Research were performed to eliminate the influence of every parameter, except one: for a constant degree of iron carburization, the constant partial pressure of water vapor, the calculations were made for a constant value of mass gain.

Nanocrystalline iron was carburized with pure methane at 660 °C to obtain different carburization degrees. Some X-ray diffraction (XRD) model patterns of nanocrystalline iron samples before reaction and catalyst samples after the carburization process are shown in Figure 1. The identified crystallographic phases are marked.

In XRD pattern of the sample after reduction only, α-Fe phase peaks can be seen. In the XRD pattern of the sample after carburization, iron carbide Fe_3C and graphite peaks are seen. No other iron carbides are created during the carburization process of iron with methane under the examined conditions. The average crystallite size of nanocrystalline iron (after passivation) calculated from the Fe(211) reflection on the basis of eq 1 was equal to 18 nm and that of iron carbide Fe_3C(200) and graphite C(002) in the sample with carburization degree equaled 1 amounting to 30 and 10 nm, respectively. The influence of carburization degree on the intensity of graphite peak C(002) expressed as the peak area is shown in Figure 2.

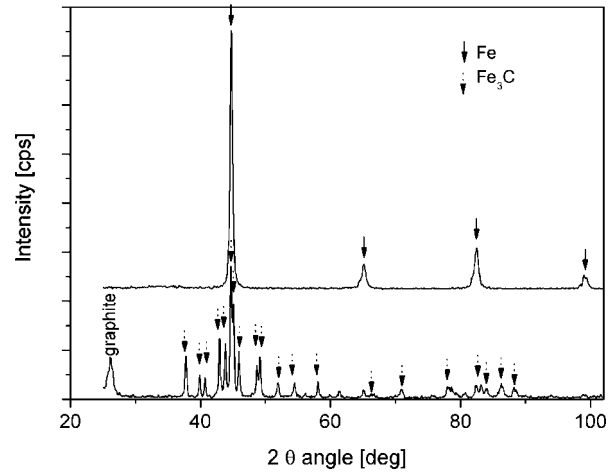

Figure 1. XRD patterns of nanocrystalline iron after the passivation process (upper) and sample after carburization with methane (bottom) (p_{CH_4} = 1 bar, T = 660 °C, m_C/m_{Fe} = 1 g of C/g of Fe).

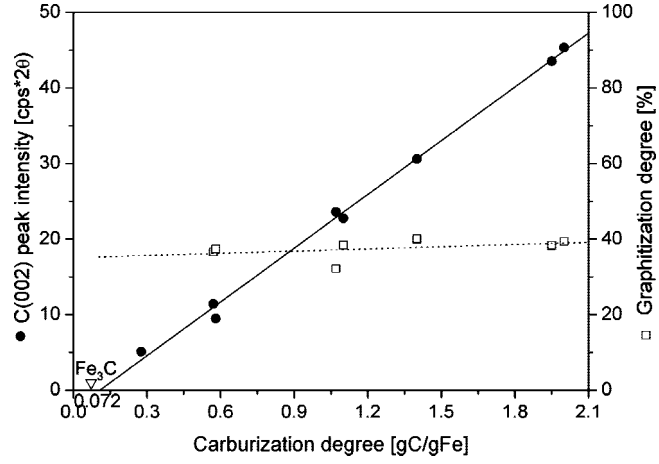

Figure 2. The dependence of intensity of graphite peak C(002) and its graphitization degree on carburization degree.

Every increase of carbon content in the samples above the value of iron carbide led to an increase of the graphite peak. The intersection of the extrapolated line with the axis of carburization degree is close to 0.075 gof C/g of Fe. This value corresponded to carbon content in the stoichiometric compound of iron carbide 0.072 g of C/g of Fe. It suggests that after completion of iron carbide formation, the graphite form creation starts (the XRD peak C(002)).

The average size of graphite crystallites was determined as 10 nm independent of the carburization degree of the samples. The graphitization degree calculated with respect to eq 2 equaled close to 40% and did not depend on the carburization degree of the samples.

The carburization process led to an increase of the size of sample grains. For example, the grain with a diameter of 1 mm increased two times for a sample carburization degree equal to 1. In Figure 3 SEM images taken of iron catalyst before and after carburization process are shown. In Figure 4 EDX spectra of area and point microanalysis of nanocrystalline iron (Figure 3a) are shown.

In the pictures taken with this resolution the smooth surface of iron, covered only with islands of structural promoters can be seen; the spectrum of EDX analysis made in the marked point supported that. The content of promoter oxides measured with microanalysis indicates their presence in a form of compounds with low reduction capacity, $CaO \cdot SiO_2$,

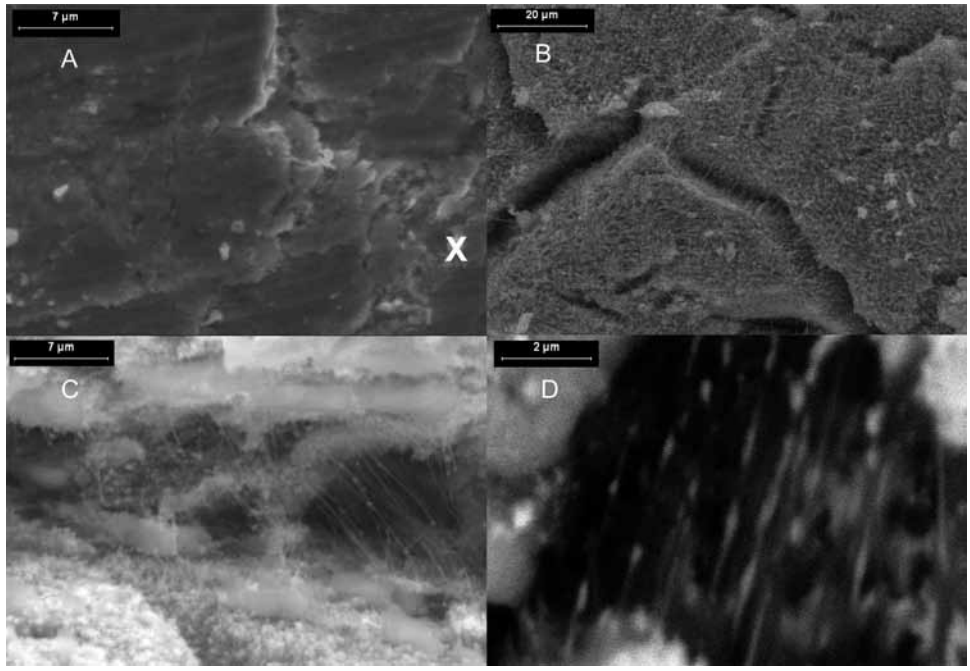

Figure 3. SEM images of nanocrystalline iron samples after (A) passivation and (B−D) carburization. The cross mark reflected the point of EDX analysis.

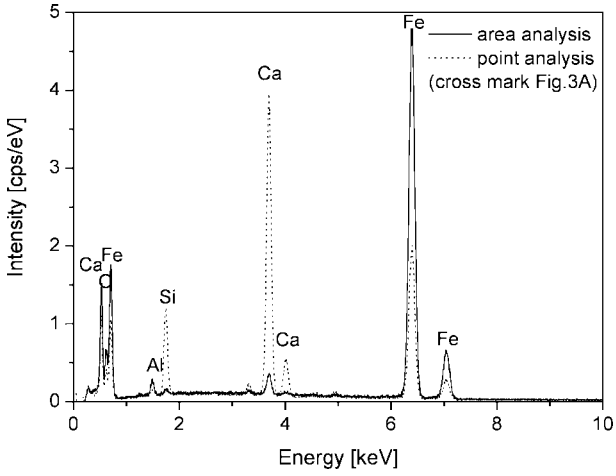

Figure 4. EDX microanalysis of nanocrystalline iron, Figure 3A.

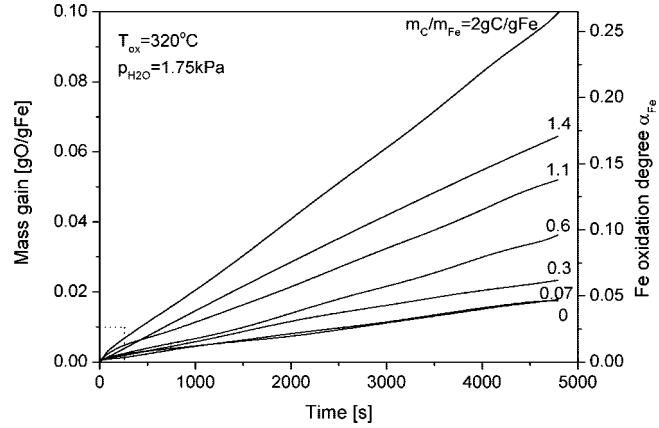

Figure 5. TG curves of the process of iron carbide oxidation with water vapor for samples with different carburization degree.

$CaO \cdot Al_2O_3$, and $CaO \cdot Fe_2O_3$. Small crystallites of iron were not yet seen, but the grain boundaries, which reflected the magnetite region in raw material, can be seen. The samples after the carburization process changed into a porous carbon sponge. The obtained carbon deposit had mainly the form of graphite and carbon wires and can be seen in Figure 3C. Figure 3D was made with back-scattered electrons technique and bright color points show the position of iron carbide in the sample. The average size of this species was determined as ∼150 nm whereas the average crystallite size of iron carbide determined with the XRD method was 30 nm. It can be concluded that iron carbide exists in the form of agglomerates. The wires during their growth extract iron carbide particles from the bulk of a grain.[20] As a result of this process, iron carbide is dispersed in a carbon matrix as agglomerates.[21,22]

The samples after carburization were oxidized in the temperature range of 300−450°C and partial pressure of water vapor of 0.63−3.26 kPa H_2O. The sample of pure carbon deposit, prepared by dissolving iron oxides in hydrochloric acid, was stable under these conditions. In the presence of iron oxides and iron, the total carbon analysis showed that the content of carbon in a sample was not changed during the process. The obtained carbon deposit started to react with water vapor at the temperature of 500 °C, and it was the upper limit of the applied temperatures.

The samples were carburized to obtain different degrees of carburization, so the mass of the samples used in oxidation was different for every experiment. Simultaneously, the quantity of iron carbide was the same for every sample. The samples were oxidized with water vapor under partial pressure of 1.75 kPa and at the temperature of 320 °C. Figure 5 shows the TG lines of samples with different degrees of iron carburization during the initial stage of oxidation. Applied in Figure 5, the term iron oxidation degree α_{Fe} is expressed as a conversion of iron into magnetite and is alternatively used with oxygen mass gain.

The investigations were performed in the region where the rate-limiting step is adsorption or surface reaction. The composition of gas mixture in the reactor was not constant at the beginning of the process. The partial pressure of water vapor increased from 0 to 1.75 kPa. The area marked in Figure 5 with

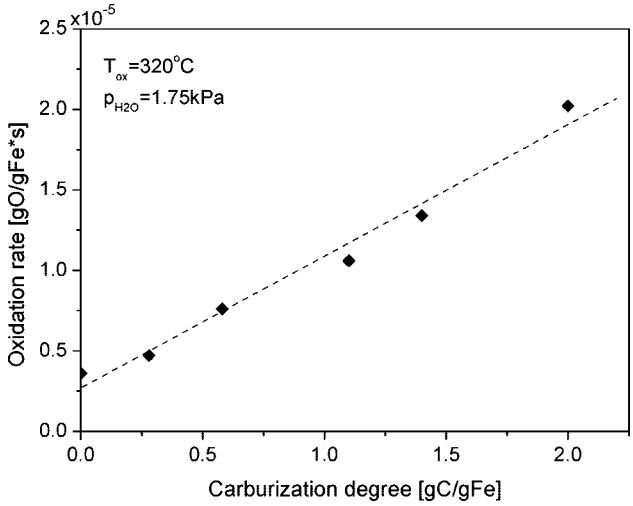

Figure 6. The dependence of the oxidation rate on carburization degree.

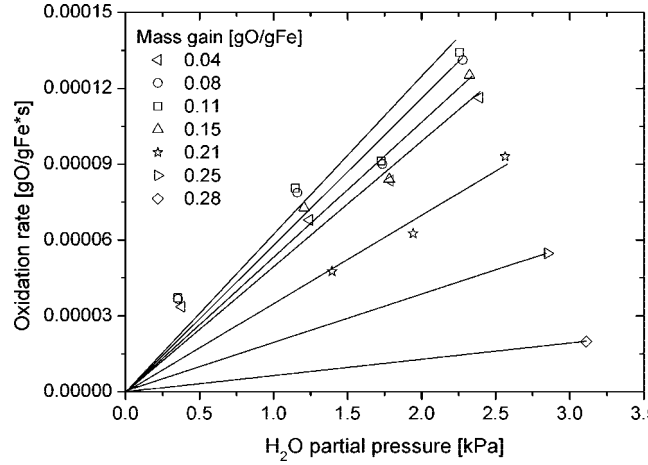

Figure 8. The dependence of the oxidation rate on partial pressure of water vapor for different mass gains.

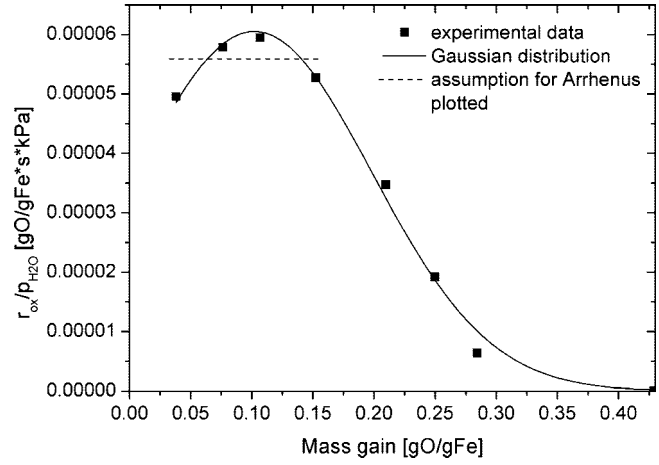

Figure 9. The dependence of the ratio of oxidation rate and partial pressure of water vapor on mass gain.

dotted lines reflected the time needed to fully fill the reactor volume with the reacting mixture. It is generally accepted that this time is expressed as the triple time needed to replace the volume of reactor. In this case it equaled approximately 200 s.

The TG lines of iron and iron carbide oxidation overlapped themselves in the initial stage of reaction. It means that both iron and iron carbide oxidize with the same rate. The carbon found in iron carbide does not affect oxidation process.

The presented TG lines can be described approximately as linear for all carbon content in the samples. It means that at an initial reaction stage the reaction rate is constant and does not depend on the iron oxidation degree. The iron carbide oxidation rate was calculated from the slope of TG lines and subsequently it was correlated with the degree of sample carburization. The obtained dependence of the reaction rate of oxidation on the carburization degree of iron is shown in Figure 6.

On the basis of the above shown dependence, it was assumed that the rate of oxidation increases linearly with the degree of iron carburization. Oxidation was taking place in the whole volume of the grain, because it is the initial stage of the process and, as it was mentioned earlier the reaction is kinetic, not diffusion limited. The size of single agglomerate of iron equals approximately 150 nm,[23] and the size of iron carbide agglomerates which can be seen as bright points in the BSE image in Figure 3D are similar. The density of them is similar now that their shape is comparable too. Iron and iron carbides are oxidized with the same reaction rate. The low content of carbon in iron carbide does not slow down the process of dissociative adsorption of water vapor on the iron surface. The rate of oxidation at the range of low carburization degree (more or less iron carbide) is affected by the form of carbon, and not by its content. The samples with a higher carburization degree have higher specific surface area on which more particles of water

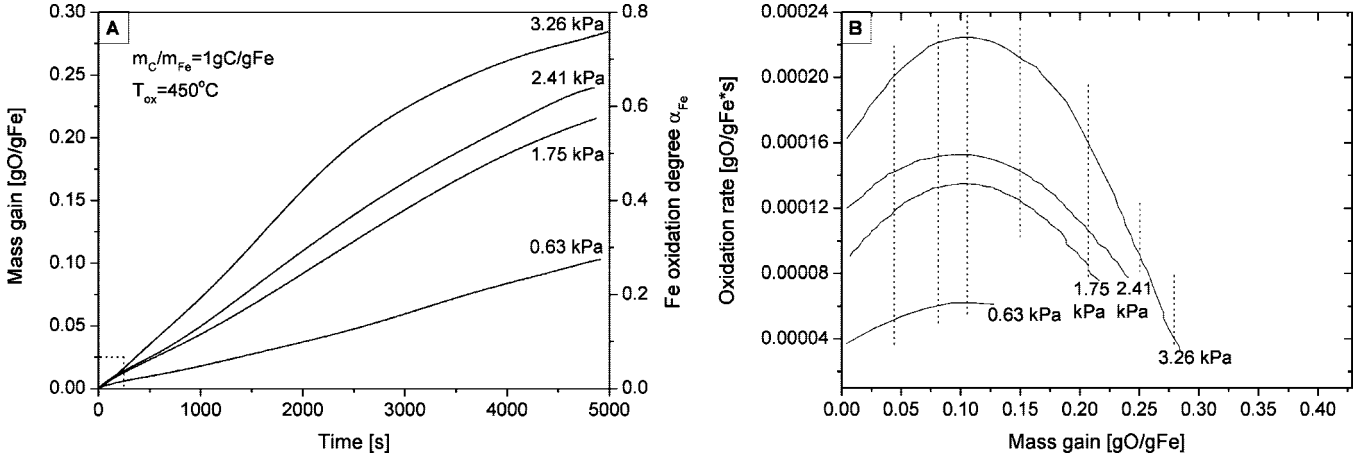

Figure 7. TG (panel A) and correlate with them DTG (panel B) curves of the process of iron carbide oxidation with different partial pressures of water vapor.

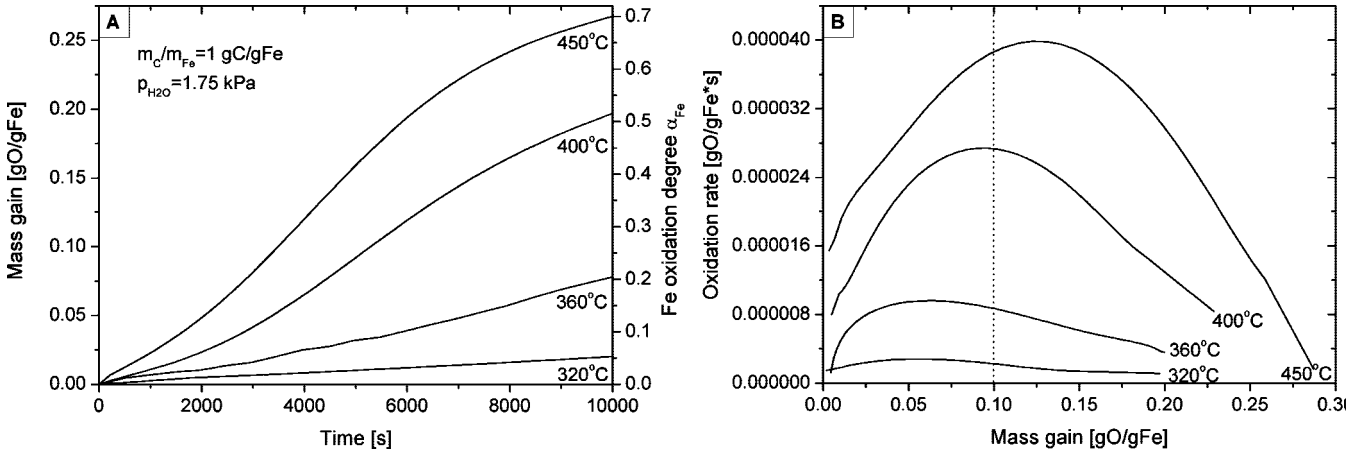

Figure 10. TG curves of the process of iron carbide oxidation at different temperatures (panel A) and correlated with DTG curves (panel B).

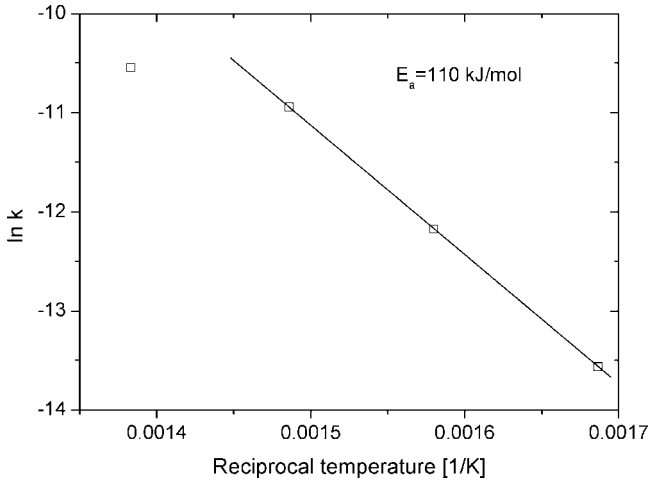

Figure 11. The dependence of Arrhenus (m_O/m_{Fe} = 0.1 g of O/g of Fe).

vapor adsorbes more easily. The increase of oxidation rate can be explained as the result of the spillover effect. According to that the particles of water vapor that adsorbed on the surface of carbon are precursors of the whole process.

The influence of the partial pressure of water vapor on the reaction rate of oxidation was tested at a constant temperature of 450 °C and for a constant degree of iron carburization which was 1 g of C/g of Fe. The TG lines obtained during the oxidation process and DTG lines correlated with them are shown in parts a and b of Figure 7, respectively.

The dependence of the reaction rate on the partial pressure of water vapor for different degrees of iron oxidation is shown in Figure 8.

The rate of oxidation increases with the partial pressure of water vapor. The dependence is linear in the examined range of the partial pressure of water vapor, so the reaction is of the first order. The linear fittings begin in the axes origin because if there is no oxidant in gas mixture, then no oxidation process occurs. Nitrogen used in experiments has very high purity, so there was no oxidation of iron carbide with contaminations.

The kinetic equation for the reaction rate has the following form:

$$r_{ox} = kp_{H_2O} \tag{3}$$

where r_{ox} is the oxidation rate and k_1 is the reaction rate constant.

On the basis of the slopes of the lines obtained in this relation, the dependence of the ratio of oxidation rate and H_2O partial pressure on the mass gain was plotted (Figure 9).

The dependence of ratio of oxidation rate and water partial pressure on mass gain exhibited a local maximum and could not be described using a simple, monotone function. In nanocrystalline materials, the crystallite size distribution can determine the reaction rate.[24] The function of Gaussian distribution was adopted, and experimental data were well compatible with it. The kinetic equation is

$$r_{ox} = kp_{H_2O}\frac{1}{w\sqrt{2\pi}}e^{-(m_O-\bar{m}_O)/2w^2} \tag{4}$$

where w is the standard deviation, m_O is the mass gain and $\bar{m}_O$ is the mass gain correlated with the ratio maximum of oxidation rate and H_2O pressure.

The influence of temperature on the reaction rate was determined by carrying out the process in a constant partial pressure of water vapor of p_{H_2O} = 1.75 kPa but at different temperatures ranging between 300 and 450 °C. At a higher temperature the carbon deposit starts to react with water vapor. The dependence of iron oxidation degree on the reaction time for different temperatures is shown in Figure 10.

The maximum rate of oxidation moves in the direction of higher degrees of iron oxidation. This effect can be a result of nanocrystalline structure of iron which has a wide distribution of crystallite size. The reaction rate was determined at the constant value of mass gain (m_O/m_{Fe} = 0.1 g of O/g of Fe). It was assumed that the ratio of oxidation rate and partial pressure of water was approximately a stable value for the range of low mass gain close to 0.15 g of O/g of Fe (dashed line in Figure 9). In this case the reaction constant rate, which is necessary to determine apparent activation energy, was calculated from eq 3.

Using these values the Arrhenus type dependence for oxidation reaction was plotted, Figure 11. The value of apparent activation energy was calculated from this dependence, and it amounted to 110 kJ/mol.

The phase composition of the samples after reaction with water vapor was determined using the XRD method. Some XRD model patterns of the reacted samples are shown in Figure 12. The identified crystallographic phases are marked.

The patterns shown in Figure 12 were obtained for the samples, which were prepared from the same raw material; the carburization degree of the presented samples was always

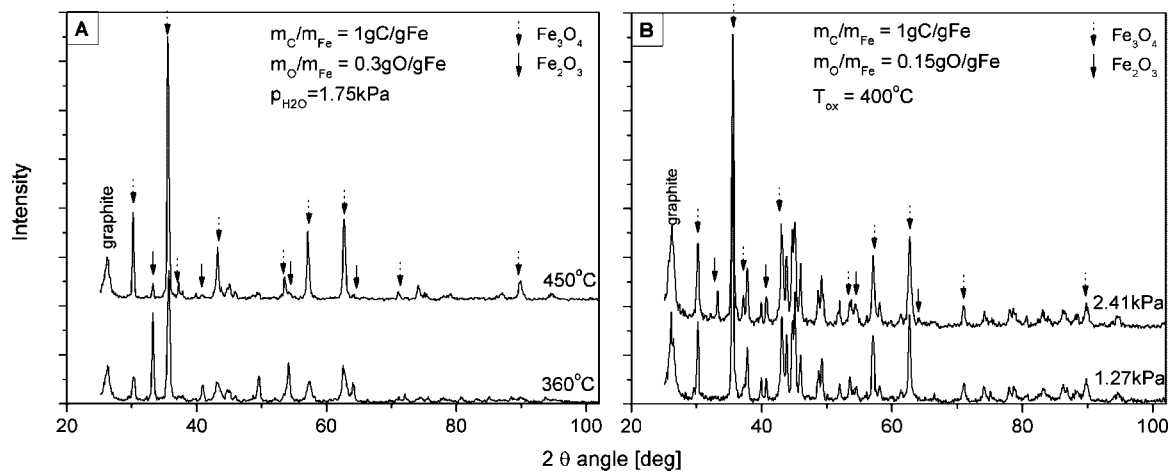

Figure 12. The influence of oxidation temperature (panel A) and partial pressure of water vapor (panel B) on qualitative phase composition of product.

m_C/m_{Fe} = 1 g of C/g of Fe. The phase composition of a sample strongly depends on the oxidation conditions: temperature and partial pressure of water vapor.

The influence of oxidation temperature on the phase composition of the product is shown in Figure 12A. The relative increase of oxygen mass obtained during oxidation was the same, and it equaled m_O/m_{Fe} = 0.3 g of O/g of Fe. The partial pressure of water vapor was p_{H_2O} = 1.75 kPa in both cases, but the temperature of oxidation varied and it amounted to either 450 or 360°C. The crystallographic phases identified in both samples were: graphite, magnetite, a small amount of hematite, and unreacted iron carbide. It can be seen that the content of hematite and magnetite is different. A sample prepared at a higher temperature has a higher content of magnetite.

The influence of partial pressure of water vapor is shown in Figure 12B. The relative increase of oxygen mass obtained during oxidation was the same m_O/m_{Fe} = 0.15 g of O/g of Fe. The temperature of oxidation was 400 °C, but the partial pressure of water vapor was different: p_{H_2O} = 1.27 and 2.41 kPa. When the partial pressure of water vapor is high, then the crystallographic phases identified in the sample are the same as above: graphite, magnetite, hematite, and unreacted iron carbide. When the partial pressure is low, the only iron oxide which can be seen in the XRD pattern is magnetite dispersed in a carbon matrix.

Oxidation with water vapor is commonly named "mild oxidation". However, hematite was formed during the process at low temperatures and high pressures of water vapor. At these conditions the rate of oxidation was low and also the consumption of water vapor in the reaction was low. Following on from that, the relation of pressures of water vapor and hydrogen, formed during the reaction, was relatively high. This relation can be named the oxidizing potential. If the oxidation rate was high, then the oxidizing potential was much lower, because more water vapor was used in the reaction and the concentration of the obtained hydrogen was higher. Should this be the case, magnetite was the main oxidation product. The reaction rate declined during the reaction route, and so did the oxidizing potential. As a result the mixture of magnetite and hematite was formed and its composition depended on the oxidizing potential of gaseous phase.

The average crystallite size of cementite, magnetite, and hematite was calculated using Scherrer's equation and it equaled 30, 40, and 60 nm, respectively. During oxidation process one small atom of carbon in iron carbide Fe_3C is replaced with four atoms of oxygen in magnetite Fe_3O_4 as a result of which crystallites grow up from 30 nm for iron carbide to 40 nm for magnetite.

Conclusions

Nanocrystalline iron carbide in a carbon matrix reacts with water vapor at 300°C and higher temperatures. The upper limit of the temperature is 500°C at which the carbon deposit starts to react with water vapor. At the initial stage of oxidation, the reaction rate increases with the degree of iron carbonization as a result of the spillover effect. The apparent activation energy equals 110 kJ/mol. Magnetite (40 nm) and hematite (60 nm) are formed during this reaction. An increase of temperature and decrease of the partial pressure of water vapor are conducive to a rise of magnetite content.

Acknowledgment. This work has been cofinanced by European Union within the framework of the European Social Fund and the Country's Budget, Human Capital Operational Programme of Priority VIII, systemic project implemented by the provincial job centre in Szczecin, "Investing in knowledge stimulates innovation in the region".

References and Notes

(1) Hacker, V.; Frankhauser, R.; Faleschini, G.; Fuchs, H.; Friedrich, K.; Muhr, M.; Kordesch, K. *J. Power Sources* **2000**, *86*, 531–535.

(2) Hacker, V.; Faleschini, G.; Fuchs, H.; Frankhauser, R.; Simader, G.; Ghaemi, M.; Spreitz, B.; Friedrich, K. *J. Power Sources* **1998**, *71*, 226–230.

(3) Hacker, V. *J. Power Sources* **2003**, *118*, 311–314.

(4) Fraser, S. D.; Monsberger, M.; Hacker, V. *J. Power Sources* **2006**, *161*, 420–431.

(5) Narkiewicz, U.; Ekiert, E.; Arabczyk, W. *Przem. Chem. (in Polish)* **2007**, *86/9*, 911–917.

(6) Chiou, W. C.; Carter, E. A. *Surf. Sci.* **2003**, *530*, 88–100.

(7) Zhao, X. Q.; Liang, Y.; Hu, Z. Q.; Liu, B. X. *J. Appl. Phys.* **1996**, *80*, 5857–5860.

(8) Bi, X. X.; Ganguly, B.; Huffman, G. P.; Huggins, F. E.; Endo, M.; Eklund, P. C. *J. Mater. Res.* **1993**, *8/7*, 1666–1674.

(9) Dong, X. L.; Zhang, Z. D.; Xiao, Q. F.; Zhao, X. G.; Chuang, Y. C.; Jin, S. R.; Sun, W. M.; Li, Z. J.; Zheng, Z. X.; Yang, H. *J. Mater. Sci.* **1998**, *33*, 1915–1919.

(10) SongH.; Chen, X. *Chem. Phys. Lett.* **2003**, *374/3−4*, 400–404.

(11) Arabczyk, W.; Konicki, W.; Narkiewicz, U. *Solid State Phenom.* **2003**, *94*, 181–4.

(12) Arabczyk, W.; Narkiewicz, U.; Ziebro J., Konicki W. PL patent P359774, 2003.

(13) Akiyama, T.; Miyazaki, A.; Nakanishi, H.; Hisa, M.; Tsutsumi, A. *Int. J Hydrogen Energy* **2004**, *29*, 721–724.

(14) Svoboda, K.; Slowinski, G.; Rogut, J.; Baxter, D. *Energy Conversion and Management* **2007**, *48*, 3063–2073.

(15) Tadashi, N.; Kenichi, Y.; Eiji, I.; Kazuo, T.; Chikanori, K.; Yasushi, S.; Keiichi, K.; Shin, K. JP patent 2004204294, 2004.

(16) Arabczyk, W.; Narkiewicz, U.; Pełech, I.; Podsiadły, M.; Ekiert, E.; Pelka, R. PL patent P384834, 2008.

(17) Jasińska, I.; Moszyński, D.; Arabczyk, W.; Kaleńczuk, R. *Pol. J. Chem. Technol.* **2003**, *5/4*, 70–72.

(18) Klug, H. P.; Alexander, L. E. *X-ray Diffraction Procedures for Polycrystalline and Amorphous Materials*, 2nd ed.; John Wiley: New York and London, 1974.

(19) Ermakova, M. A.; Ermakov, D. Y.; Chuvilin, A. L.; Kuvshinov, G. G. *J. Catal.* **2001**, *201*, 183–197.

(20) Narkiewicz, U.; Arabczyk, W.; Pełech, I.; Guskos, N.; Typek, J.; Maryniak, M.; Woúniak M, J.; Matysiak, H.; Kurzydłowski, K. J. *Mater. Sci* **2006**, 1067–1075.

(21) Narkiewicz, U.; Guskos, N.; Arabczyk, W.; Typek, J.; Bodziony, T.; Konicki, W.; Gąsiorek, G.; Kucharewicz, I.; Anagnostakis, E. A. *Carbon* **2004**, *42/5−6*, 1127–1132.

(22) Guskos, N.; Anagnostakis, E. A.; Gasiorek, G.; Typek, J.; Bodziony, T.; Narkiewicz, U.; Arabczyk, W.; Konicki, W. *Mol. Phys. Rep.* **2004**, *39*, 58–65.

(23) Schlögl, R. In *Catalytic Ammonia Synthesis, Fundamentals and Practice*; Jennings J. R., Ed.; Plenum Press: New York, 1991; pp 19−108.

(24) Wróbel, R.; Arabczyk, W. *J. Phys. Chem. A* **2006**, *110*, 9219–9224.

JP809518B